Journal of Applied Physics

Crack quasi-healing in films of vertically aligned 1D nanostructures: Impact of compliance in a 1D geometry

Cite as: J. Appl. Phys. **131**, 164701 (2022); https://doi.org/10.1063/5.0086061
Submitted: 21 January 2022 • Accepted: 02 April 2022 • Published Online: 22 April 2022

Ludovic Pauchard, Frédérique Giorgiutti-Dauphiné and David McIlroy

AIP Publishing

Journal of Applied Physics ARTICLE scitation.org/journal/jap

Crack quasi-healing in films of vertically aligned 1D nanostructures: Impact of compliance in a 1D geometry

Cite as: J. Appl. Phys. **131**, 164701 (2022); doi: 10.1063/5.0086061
Submitted: 21 January 2022 · Accepted: 2 April 2022 ·
Published Online: 22 April 2022

Ludovic Pauchard,[1,a)] Frédérique Giorgiutti-Dauphiné,[1] and David McIlroy[2]

AFFILIATIONS

[1]Université Paris-Saclay, CNRS, FAST, 91405 Orsay, France
[2]Department of Physics, Oklahoma State University Stillwater, Stillwater, Oklahoma 74078, USA

[a)]**Author to whom correspondence should be addressed:** ludovic.pauchard@universite-paris-saclay.fr

ABSTRACT

We study nanostructured films made of helical nanowires and nanosprings, which provide remarkable mechanical behavior. When subjected to wetting and drying processes, these films crack like most coatings. However, beyond the great ability of these films to shrink, the cracks partially close when these films are no longer mechanically stressed. While for conventional coatings about 20% of the crack opening is relieved, more than 80% of the crack opening is relieved in films of nanosprings when the film is unloaded. We show here that this quasi-reversibility is related to (i) the high compliance of the material, (ii) the low energy consumed by plasticity, and (iii) the high deformability of the film components, e.g., the nanosprings. These results are compared to the case of usual particulate films.

I. INTRODUCTION

Nanostructured materials have attracted considerable attention in both academic and industrial circles in the past decade due to their potential applications in fields such as chemical sensors[1,2] and optoelectronic devices.[3,4] In particular, they exhibit widely adjustable mechanical properties, which provide promising applications in biointerface materials that can guide the design of synthetic materials for tissue engineering and healing. Among the emerging group of nanostructures, helical nanowires, e.g., nanosprings, are multiple functional nanomaterials.[5,6] A key question concerning these materials is how failures develop. In this context, we address the formation of cracks in successively stressed compliant nanospring films. In general, crack patterns depend on the applied stress and the way the material releases it. The cracks, thus, present geometrical characteristics described by the following parameters: depth, thickness, density, spacing, and aperture. In this way, the crack pattern reveals the mechanical properties of the material[7] and offers a wide variety of applications.[8,9] These patterns have been extensively observed in a variety of materials, such as ceramics, paints, or particulate coatings, where cracking results from solvent evaporation.[10–15] In the last, capillary forces produced by the surface tension of the solvent are sustained by the wet structure. Therefore, the mechanical response of the structure determines the ability of the material to release the stress through significant overall shrinkage or cracking. For particulate coatings, after drying is complete, cracks close to less than 20% of their initial opening or remain opened, which attest to plastic behavior.

In this article, we consider here films of Vertically Aligned NanoSprings (VANS) that is a highly porous material bonded to a stiff substrate. The formation of cracks in these nanostructured films shows specific characteristics compared to conventional brittle coatings such as colloidal coatings. Indeed, these compliant films that are stressed by wetting and drying present a high ability to shrink. The resulting cracks exhibit a large opening, then close over more than 80% of their initial opening when the film is unloaded (Fig. 1). This quasi-healing is due to several characteristics as evidenced in this article. On the scale of the film, the compliance of the film has been highlighted through nanoindentation testing. Moreover, considerations based on an energy balance provide an estimation for the weak energy plastically consumed in the films during the opening/closing of the cracks. This points out the remarkable dominance of film elasticity. On the scale of film components, the high deformability of the individual nanosprings is supported by their flexible and elongated shape. Moreover, the

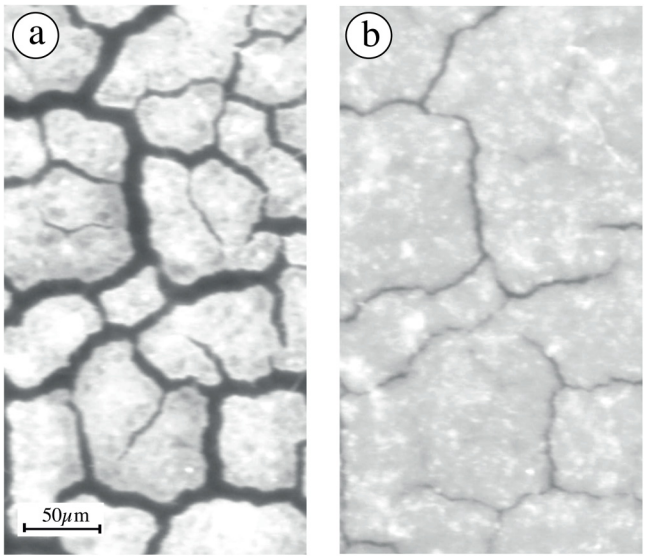

FIG. 1. Drying-induced cracks: maximal crack opening (a) then closure (b). Some cracks heal completely at the microscopic scale.

mechanical stability of the films has been highlighted through cyclic loading and repeated wetting/drying processes. These physical properties are significantly different from those of the usual particulate materials. These results support the idea that VANS have extraordinary mechanical properties and, hence, are a particularly promising system for biomimetics, utilizing a combination of nanospring coating with specific materials.

II. EXPERIMENTAL

A. Nanosprings synthesis

The nanospring film consists of an array of helical silica nanowires aligned perpendicularly to the substrate surface, e.g., Vertically Aligned NanoSprings (VANS), as shown in Figs. 2(a) and 2(b). We synthesize the helical nanowires via a modified Vapor–Liquid–Solid (VLS) mechanism on a Si substrate. A detailed description of the nanospring growth process can be found in references by McIlroy *et al.*[16] and Wang *et al.*[6] The highly dense array of nanosprings is due to the density of particles sputtered onto the Si substrate and serving as the catalyst for the VLS process. The areal density is estimated at $m = 5 \times 10^{10}$ nanosprings per cm^2 using SEM micrographs.[17] In turn, the helical nanowires growth uses catalytic liquid droplets at the tip of the nanowires. The catalytic particle adsorbs the molecules of the vapor and then diffuses toward the particle–nanostructure interface. A controlled asymmetry leading to an anisotropy in the contact angle at the catalyst droplet–nanowire interface is responsible for a torque of the droplet.[5] This process results in the formation of a helical structure. The thickness of the nanospring film was varied by controlling the growth rate of the nanospring on the substrate. In this way, the measurements are carried out on films with a thickness of 8, 14, and 26 μm. The cohesion of the vertically aligned nanosprings in the film is ensured by chemical bonding SiO_x–SiO_2, x = 1–2.[18] Hence, the order of magnitude of the surface energy for VANS in the air is estimated to be $0.5\,J/m^2$. This results in a structural coating.

B. Mechanical properties characterization

1. Global elastic response

The mechanical response of the nanospring films is examined using nanoindentation testing (Anton-Paar). The method consists

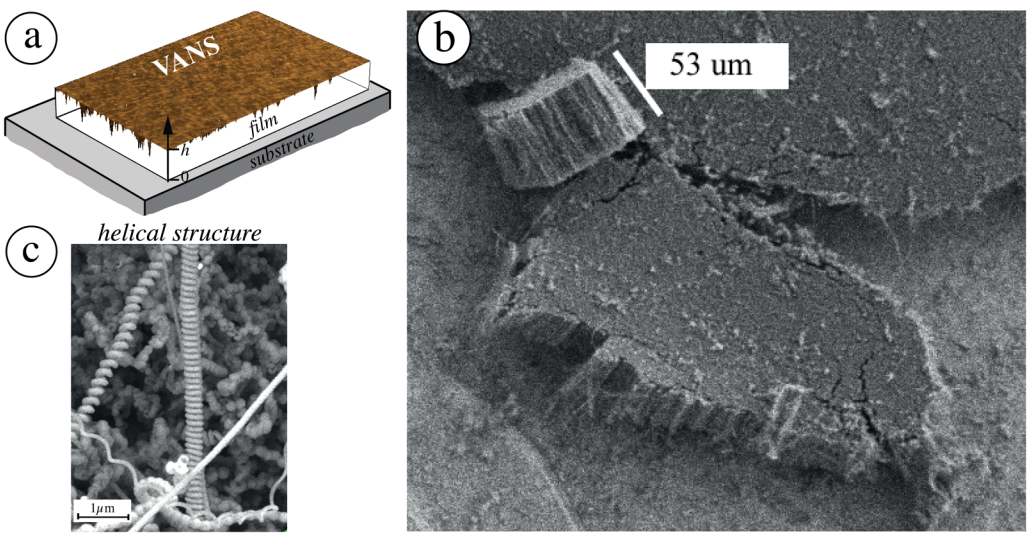

FIG. 2. (a) A schematic representation of a film of Vertically Aligned NanoSprings (VANS) on a Si substrate. (b) Scanning Electron Microscopy micrographs of a film of VANS and (c) individual nanosprings.

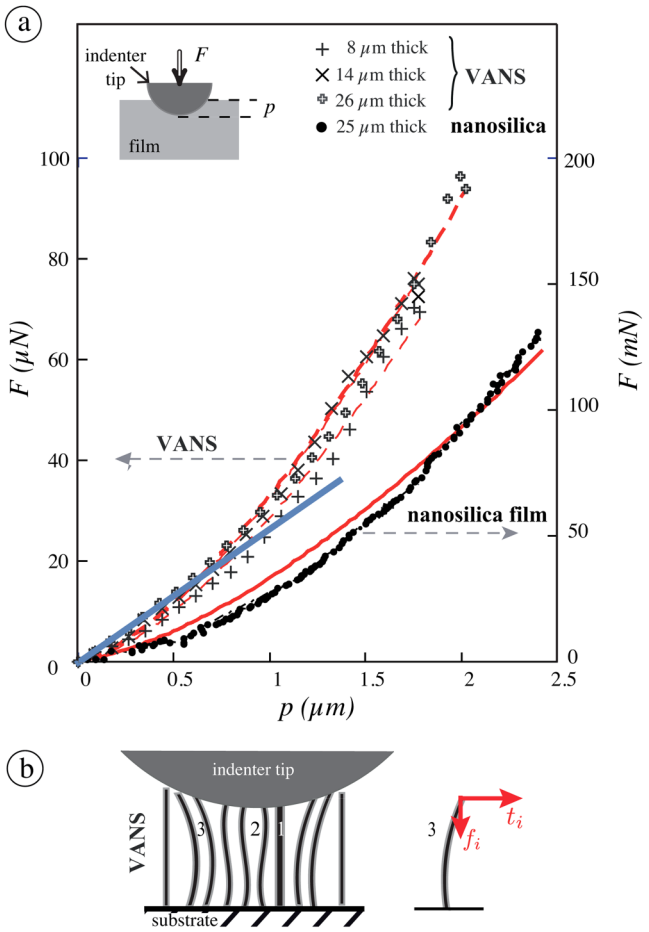

FIG. 3. Mechanical behavior using indentation testing. (a) The load, F, applied to materials is plotted as a function of the penetration depth, p, of the indenter tip. Measurements were carried out on VANS exhibiting three film thicknesses (8, 14, and 26 μm) and on a silica film (LUDOX-HS40) of 25 μm thick. The red lines are the theoretical predictions in accordance with the Hertz contact law. The blue line is the theoretical predictions in accordance with Eq. (2) for VANS. (b) Schematics of consecutive contacts of the indenter tip and nanosprings: bending deflection at the tip of the nanospring i resulting from indentation force f_i and lateral force t_i. Different events can take place: compression (1), buckling (2), and bending under the effect of the forces in red (3) (the bonds between wires are not illustrated).

of driving a spherical tip into the sample with a controlled force, F [see the sketch in Fig. 3(a)]. The range of applying loads lies from ~1 up to 100 μN. The spherical tip of radius $R = 200\,\mu$m assumed to be perfectly rigid is initially in contact with the surface of the film. Then, the tip is driven inside the sample with a controlled loading speed of 100 mN/min until a maximum load is reached.

The standard procedure of Oliver and Pharr[19] to estimate the elastic modulus from the indentation load-displacement curve uses the initial slope of the unloading curve upon unloading as the material recovers elastically (see Fig. 4 of the supplementary material). In the following, we measure the elastic behavior of the material due to an axial compression using the following process. The applied force is measured as a function of the penetration depth, p, of the indenter tip in the material. This method is a way to extract the average value of the elastic modulus, E, of the coating. Measurements are reported in Fig. 3(a) for films of VANS at various thicknesses. The loading curves are well fitted by the Hertz contact law revealing the elastic behavior of the material due to an axial compression,

$$F = \frac{4\sqrt{R}}{3(1-\nu^2)} E p^{3/2}, \tag{1}$$

where ν is Poisson's ratio of the film. This technique provides measurements of the film's compressive axial stiffness but does not take into account the anisotropy of the mechanical properties of the helical structure: the stiffness was found to be 4–5 times larger in the vertical direction than in the horizontal one.[20] Thus, the average value of the vertical stiffness of the nanospring films is estimated to be $E_{VANS} = 2.34 \pm 0.18$ MPa based on the curve fitting using Eq. (1) ($\nu = 0.27$[21]). This low value indicates that the nanospring films exhibit compliant properties, where minor stress is required for a considerable strain. Note that the film thickness barely influences the measurements.

The stiffness of the nanospring films is compared to that of a particulate coating: in particular, the drying of dispersions of charged silica nanoparticles (LUDOX-HS40 commercially available from Sigma-Aldrich with a particle size of 12 μm) leads to solid films whose stiffness, E_{silica}, is obtained using microindentation testing (CSM Instruments Micro Indentation Tester, MHT with a range of applying loads lies from ~20 mN up to 10 N) as shown in Fig. 3(a). The loading curve fitted using the Hertz contact law gives $E_{silica} = 1.5 \pm 0.3$ GPa (using $\nu = 0.18$[22]).

Besides, the reproducibility of the mechanical response was analyzed through repeated indentation tests as shown in Fig. 4(a). In the case of nanospring films, the cyclic loading between loaded 400 μN and unloaded states 200 μN results in a cyclic penetration depth at a loading rate of 1000 μN/min. No changes in the average indentation depth are captured in each indentation cycle: the cyclic loading results in a cyclic penetration depth at a constant load repetition. This mechanical response of the film is only observed when the delay between load/unload cycles is not too short (>5 s), in which case the average penetration depth into the material monotonously increases during the cycles (see the supplementary material). The mechanical response of the nanospring film is changed with loading frequency, suggesting a relaxation process of the individual nanosprings.

However, in the case of the particulate coating, the penetration depth monotonously increases during the cyclic indentation load, which underlines the inelastic characteristics of the particulate film under repeated loading. These results on nanosilica films are consistent with measurements obtained in other particulate films made of different silica particles as well as stiff latex particles. The resulting elastic moduli are reported in Fig. 4(b) as a function of the number of cycles. Here, we use the standard procedure of Oliver and Pharr[19] to estimate the elastic modulus as the material recovers elastically at the beginning of the unloading process.

Hence, these results confirm the mechanical stability of nanospring films under repeated loading.

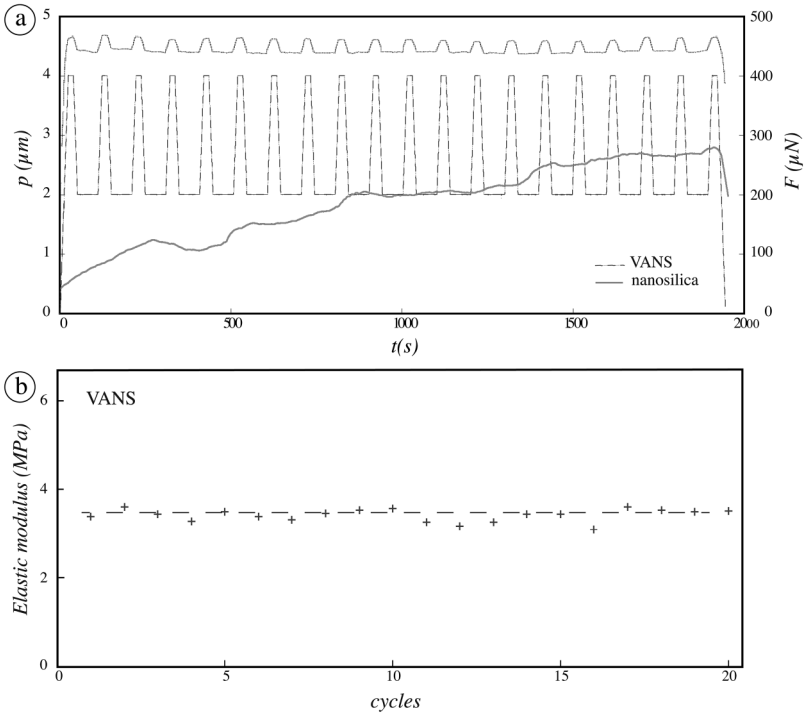

FIG. 4. (a) Time dependence of the indentation depth, p, under a cyclic indentation load, F, for a nanospring film, 26 μm thick, and for a film made of nanosilica particles (LUDOX-HS40, ~25 μm thick). (b) The resulting elastic moduli are plotted following each load/unload cycle for the nanospring film. The elastic moduli are estimated using the standard Oliver and Pharr procedure[19] (see the supplementary material). The dashed line is a guide for the eyes.

2. Individual elastic contribution of nanospring

The above investigations allow us to obtain the global elastic response of nanospring films. However, the results do not account for the individual elastic contribution of nanosprings. In this way, the following considerations are carried out to estimate the stiffness of individual nanosprings. The mechanical response of nanospring films involves different processes such as axial compression, buckling, or bending of nanosprings as sketched in Fig. 3(b). This was particularly investigated in the case of a forest of pillars in Ref. 23. In the case of nanospring films, no changes characterizing the transition between compression and buckling of nanosprings can be captured apart from indentation curves in Fig. 3(a). Moreover, since axial compression rapidly requires a significant amount of elastic energy during the loading process, the buckling or bending process preferentially contributes to the deformation of the film. Assuming that bending is the most likely deformation due to the lateral forces, t_i, acting on nanosprings [Fig. 3(b)], the total indentation force, F, can be related to the stiffness of individual nanosprings, E, through the classical nonlinear beam theory. By integration over the contact area A between the indenter and the film, it becomes[23]

$$F = \int_A \frac{\pi^2 E}{4h^2} m \left(1 - \frac{1}{(1 + (p - p_i)R^2/(h.r_i^2))^{1.15}}\right) dA_i, \qquad (2)$$

where h is the nanospring length (film thickness), p_i is the indentation depth of the nanospring i at a distance r_i from the axis of symmetry of the indenter, and $dA_i = 2\pi R dh_i - 2\pi r_i dh_i$.

Considering $h = 26\,\mu$m, the curve fitting by Eq. (2) at low penetration depth, p, gives $E = 0.20 \pm 0.04$ TPa [Fig. 3(a)]. The last value is close to the order of magnitude obtained in Ref. 20. Note that this value is barely modified if we consider the case of buckling of the nanosprings instead of bending.

III. RESULTS AND DISCUSSION

A. Wetting films of nanospring

An important specificity of nanospring films lies in the high porosity of the system.[24] To capture the permeability of the system, the process of drop imbibition in the film has been carried out. When a water drop is deposited on the surface of the nanospring surface, the drop keeps a spheroidal shape due to the air pockets trapped underneath (see Fig. 5 in the supplementary material). However, a droplet of a low-surface-tension liquid (ethanol) spreads and rapidly soaks into the nanospring film [Fig. 5(a)]. Measuring the time variation of the drop imbibition is a simple way to estimate the voids size, a, between the nanosprings. In general, the fluid flow through nanoporous materials can be described by the Washburn equation that enables to obtain the time variation of the radius, $\rho(t)$, of the wetted region as[25]

$$\rho(t) = (\gamma_{lv} a \cos(\theta)/(2\eta))^{1/2} \sqrt{t}, \qquad (3)$$

where γ_{lv} is the liquid–vapor interfacial tension, η its viscosity, and θ is the contact angle of the liquid with the solid material.

The adjustment of the measurements with Eq. (3) at the first moments of the imbibition process allows us to obtain an order of

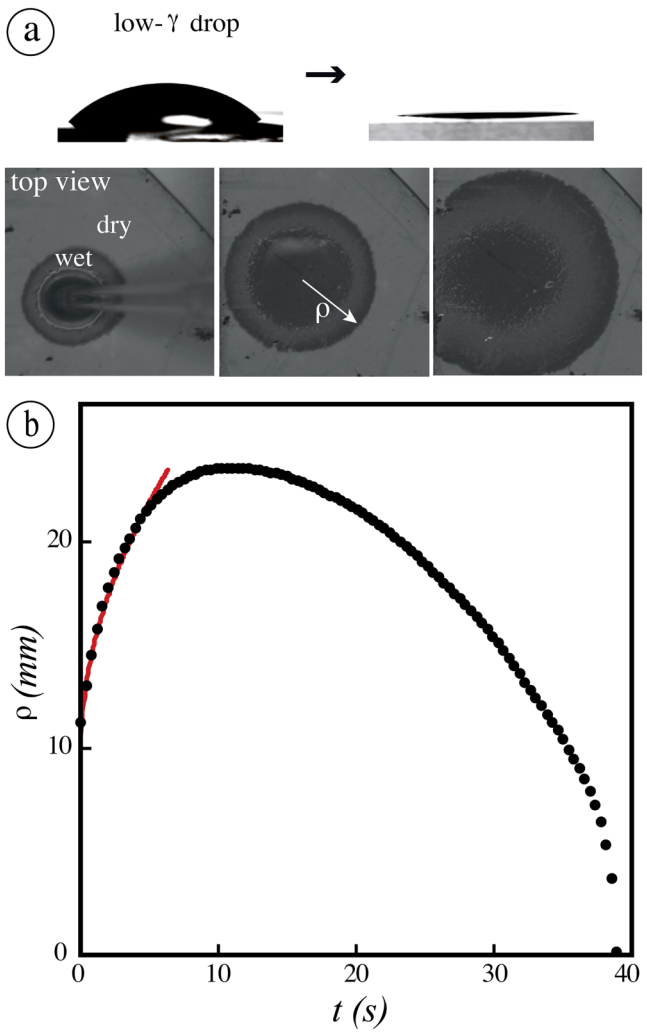

FIG. 5. (a) Wetting on a film of nanosprings. Deposition/spreading/imbibition of a drop of a low-surface-tension solvent (ethanol) into VANS (side and successive top views). (b) The radius, ρ, of the wetted region is plotted as a function of time: the time increase of ρ corresponds to the imbibition process [the line is the best fit using Eq. (3)], while the time decrease of ρ is characteristic of the evaporation of the solvent.

magnitude of the voids size of about one hundred nanometers [Fig. 5(b)]. These experiments were reproduced on three films of different thicknesses as reported in Table I.

B. Cracks induced by drying of wetted nanospring films

Evaporation of the volatile liquid from a wet porous film generally results in the formation of cracks. Cracking is caused by strong capillary forces assisted by the inherent elasticity of the film. In this way, evaporation forms pinned menisci at the liquid–vapor

TABLE I. Order of magnitude of the voids size estimated by the measurements of liquid imbibition in nanospring films (VANS). Three film thicknesses have been considered.

	VANS		
Film thickness h (μm)	8	14	26
Effective size a (nm)	95 ± 15	118 ± 12	110 ± 9

interface. The surface tension of the solvent causes a pressure difference, $\Delta\mathcal{P}$, at the evaporation surface with respect to the vapor pressure (Fig. 6). According to the Young–Laplace equation, this pressure difference is expressed as $\Delta\mathcal{P} = \frac{2\gamma_{lv}\cos(\theta)}{\mathcal{R}}$, where $\mathcal{R}$ is the radius of curvature of the menisci. As a result, the capillary pressure causes the network of nanosprings to collapse and the film to shrink at the evaporation surface.[24,26] The shrinkage is related to the nanosprings deflection whose displacement, δ, is determined by

$$\delta = \frac{\mathcal{F}h^3}{8\mathcal{E}I}, \tag{4}$$

where $\mathcal{F} = \Delta\mathcal{P}hd$ is the capillary force acting on the nanosprings and $I = \pi d^4/64$ is the cross-sectional second moment of a single nanospring assimilated to a wire of diameter d. The deflection results in the aggregation of the wires.[27]

This mechanism results in the aperture of the film that scales as $w \sim 2\delta$ as sketched in Fig. 6. Considering an average diameter $d = 10\,\text{nm}$ of a $h = 26\,\mu\text{m}$ long nanospring and elastic modulus $\mathcal{E} = 0.20 \pm 0.04\,\text{TPa}$, the capillary pressure associated with $\mathcal{R} \sim w$ is estimated at 3 kPa leading to a film aperture of $25\,\mu\text{m}$, which is consistent with the measurements from images in Figs. 1 and 7. This process governs the formation of cracks in the film (Fig. 7). The cracks invade the plane of the film to release the residual stress. Hence, crack formation is governed by the combination of three classical processes:

- nucleation: cracks nucleate at some defects [Fig. 7(b)];
- crack opening; and
- propagation. The cracks do not form simultaneously but provide a degree of hierarchy: this is particularly the case in Fig. 1 where the first crack to form is wider than the second and the third generation.[28]

Finally, the morphology of cracks shows a partial branched network whose topology is characterized by junctions and dead ends [Fig. 7(a)].

At the final stage of the drying, the film is unloaded and the capillary force F is reduced to 0. As a result, the deflection is canceled and the cracks close up.

These features are commonly encountered in the formation of cracks induced by the drying of particulate films: the shrinkage at the drying face is constrained by the adhesion of the film to the substrate. As a result, differential shrinkage is governed by the variation of liquid pressure in the pores and results from a stress distribution within the film. In the following, we focus on the crack aperture.

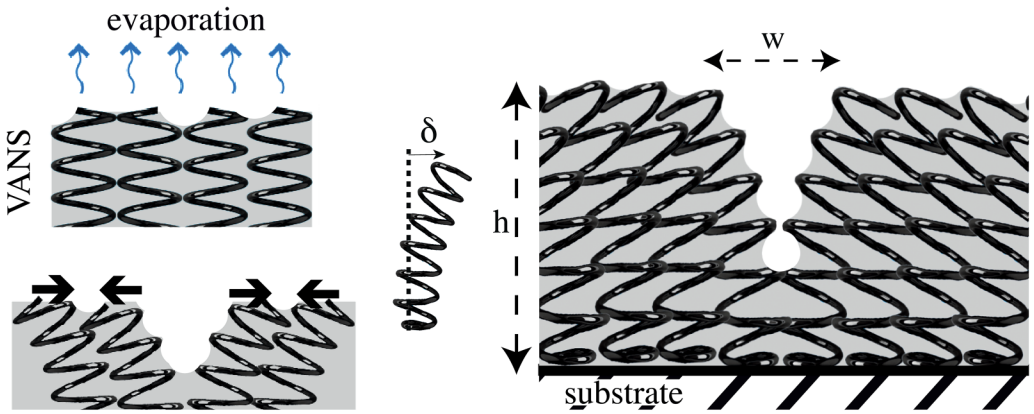

FIG. 6. Drying. Sketch in side view illustrating the crack opening induced by capillary shrinkage. Deflection δ of a single nanospring. Crack opening, w, in a network of nanosprings.

C. The impact of compliance on crack quasi-healing in nanospring films

The time variation of the crack opening then closure induced by a wetting/drying process is reported in Fig. 8. The crack opening strongly evolves during the drying process as shown in Fig. 9(a). The measurements of the crack opening, w, are correlated to the time variation of the evaporation rate, V_D, which is deducted from the film mass variation with time during the drying [Fig. 9(b)]; $t_D = h/V_D$ corresponds to the drying timescale. In the first stage, the crack widens during a drying period characterized by a constant evaporation rate. This holds for brittle colloidal films, as shown in the plot corresponding to a nanosilica film in Fig. 9(a). Crack opening results from the buildup of the drying stress in the porous film.[29] Thus, the dynamics of the crack opening appears to be well-controlled by the drying process. The crack opening stops at a maximum value (image 1 for VANS in Fig. 9). This maximum value is related to the mechanical properties of the film[29] and appears to be much higher in the case of VANS than in the case of

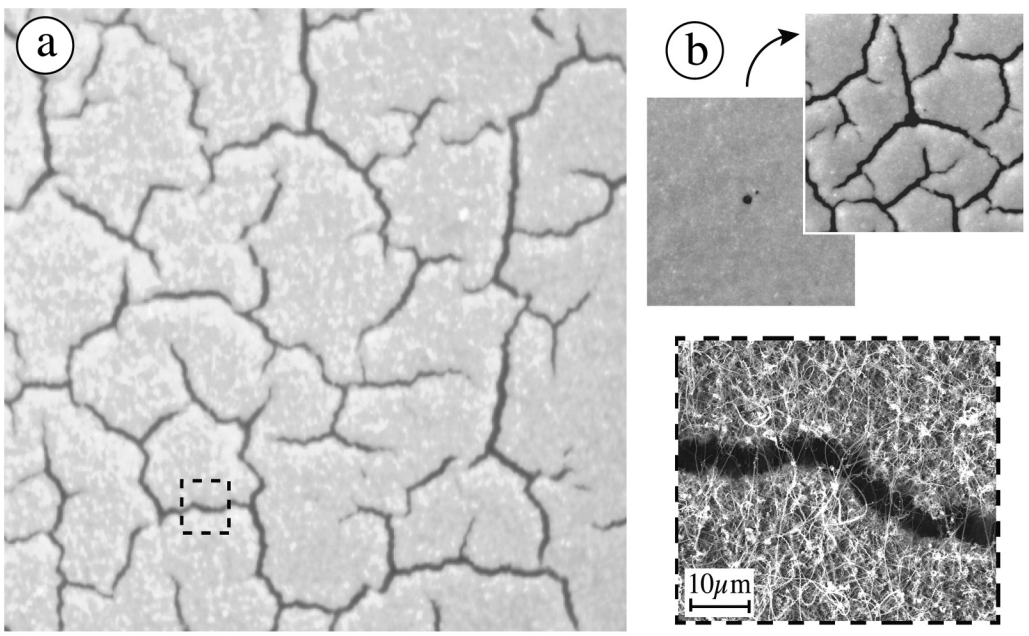

FIG. 7. (a) Branched network of cracks induced by drying a wet film of nanosprings (image width = 500 μm; film thickness = 26 μm); a Scanning Electron Microscopy micrograph is shown in the dashed square. (b) Star-like patterns with three-branched cracks nucleated from a nucleation site.

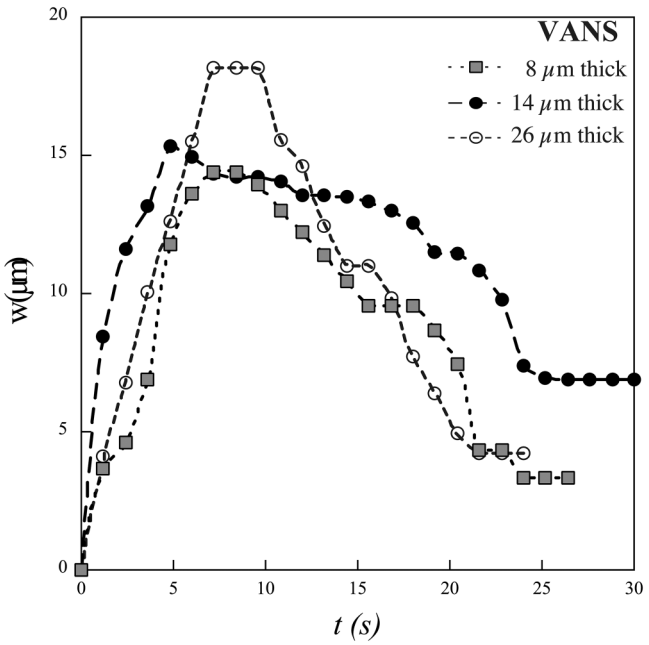

FIG. 8. Time variation of the crack opening then closure induced by a wetting/drying process. Three film thicknesses are shown.

common particulate materials. This reveals a much greater capacity for shrinkage for nanosprings than for nanoparticle gels. At a point, the drying process ceases, which is highlighted by the jump of the evaporation rate, as shown in Fig. 9(b). As the liquid located within the porous structure evaporates, the pores become empty by modifying the refractive index of the film (as evidenced by the change in the shade of gray in images 1 and 2 in Fig. 9). The consequence of the sudden decrease in the evaporation rate is that the tensile drying stress vanishes and cracks close up as a result of the elastic response of the film (images 2 and 3 in Fig. 9). At the final stage, the crack opening is noted w_p.

Whether or not the closure is complete, we observe, on average, that more than 80% of the crack opening is reversible for VANS, while less than 20% of the crack opening is relieved for usual brittle coatings. Indeed, the ratio between the maximum value of the crack opening and the reversible part of the crack displacement, $w - w_p$, is shown in Fig. 10 for a variety of films. The different materials are presented by their compliance defined as $C = E^{-1}$ that attests to the ability of deformation. In general, the irreversibility of the crack closure results from the plastic deformation of the material. The following considerations, based on an energy balance, compare the energy plastically consumed in VANS and in nanosilica coatings through the measurements of the crack opening/closure. In pure tensile loading, the crack opening may be written as

$$w \sim \frac{K_c}{E} l^{1/2}, \tag{5}$$

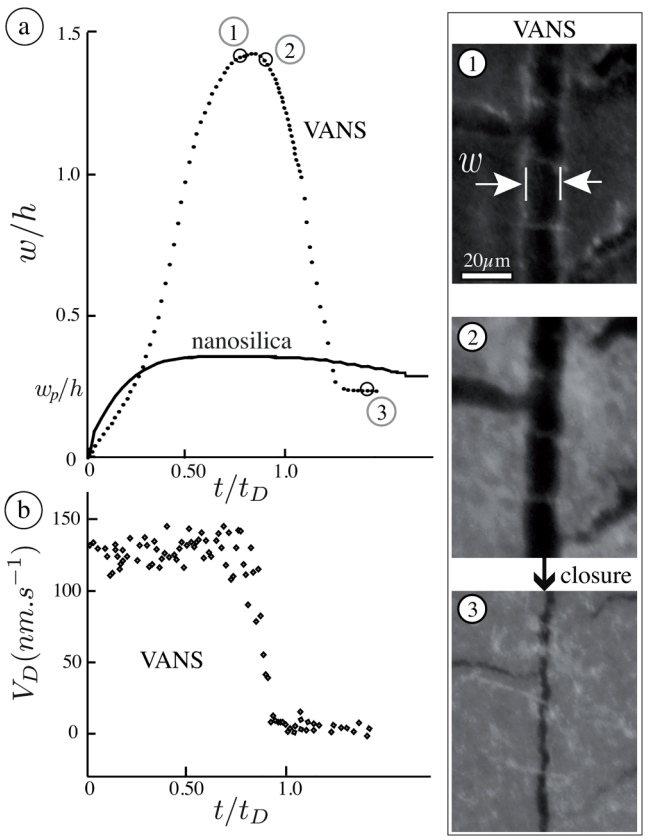

FIG. 9. (a) Typical crack opening and closing induced by the drying of wet films. The time variation of the crack opening, w, over the film thickness, h, is reported in the case of VANS (dots) and a nanosilica film (plain line); t_D is the drying timescale, which is proportional to the film thickness. Measurements were performed on the same crack. In the case of VANS, the film, 26 μm thick, is wetted by surfactant-enhanced water. The value of the opening when the drying process ceases is noted w_p. The corresponding images of a crack in VANS are labeled as 1, 2, 3. (b) Time variation of the drying rate, V_D, deduced from mass variation with time of a wet film of VANS.

where l is the distance along the crack from its tip and K_c is the critical stress intensity factor that designates the minimum stress intensity required to get an existing crack to propagate:[30] $K_c = \sqrt{G_c E}$, where G_c is the energy release rate. The energy balance states that the energy release rate is the sum of the work (or surface energy), W, used to create the new crack surfaces and the irreversible energy, U_p, due to plastic losses. The reversible part of the crack displacement, $w - w_p$, involves the reversible work W used to create the new surfaces in an ideal material without plastic losses ($U_p = 0$). Thus, Eq. (5) gives the ratio between the crack opening and the reversible part of the crack displacement as follows:

$$w/(w - w_p) = (1 + U_p/W)^{1/2}. \tag{6}$$

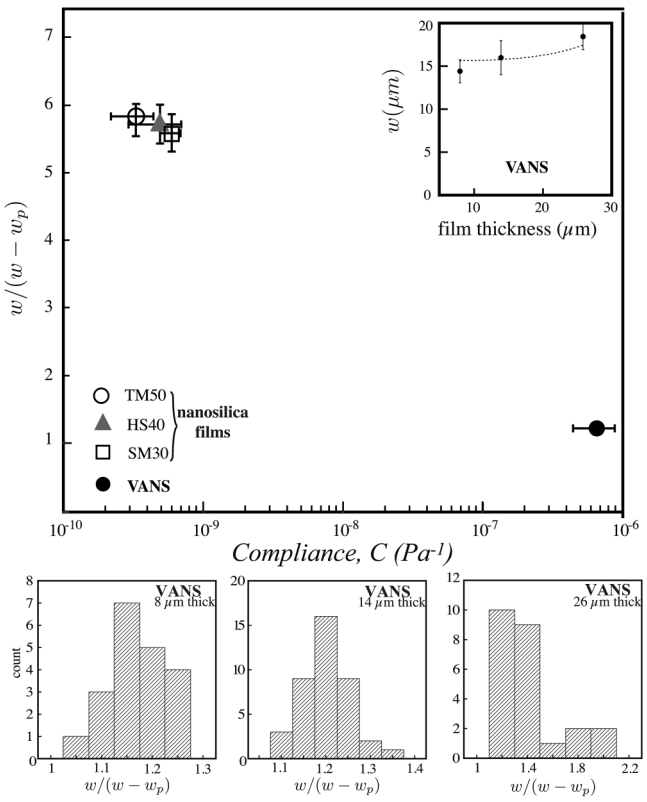

FIG. 10. Ratio between the crack opening, w, and the reversible part, $w - w_p$, of the crack displacement as a function of the film compliance, $C = E^{-1}$, in semi-log scale. Nanosilica films are obtained by the drying of aqueous suspensions of silica particles whose size is 7 nm (Ludox SM30), 12 nm (Ludox HS40) and 22 nm (Ludox TM50). Inset: mean crack opening vs film thickness [the dashed line is the best fit by Eq. (6)]. Statistics on $w/(w - w_p)$ for nanospring films of various thicknesses: the mean value is 1.16 $\pm$ 0.06, 1.20 $\pm$ 0.05, and 1.37 $\pm$ 0.23 for 8 μm thick, 14 μm and 26 μm thick, respectively. The black dot in the graph combines these different mean values.

A similar equation was obtained by Goehring *et al.*[14] Note that this analysis assumes that a crack is opening in a uniform material with uniform field tensile stress.

The order of magnitude of the surface energy for nanosilica films, W^{silica}, is estimated to be twice the surface tension of the solvent (water) for the nanosilica films: $\sim 0.14\,\text{J/m}^2$[11] while for VANS $W^{VANS} \sim 0.5\,\text{J/m}^2$ for VANS.[18] Hence, the measurements reported in Fig. 10 together with Eq. (6) allows one to estimate the irreversible energy consumed during the opening/closure of drying cracks in VANS, $U_p^{VANS} = 0.05 \pm 0.01\,\text{J/m}^2$, much lower than that for typical nanosilica films, $U_p^{\text{silica}} = 4.0 \pm 0.5\,\text{J/m}^2$.

Among the different origins of plasticity in the nanospring films, the following events can be outlined: changes in the microstructures, the modification of the bonds between nanosprings, plastic deformation of nanosprings beyond their yield strength as observed, or irreversible entanglement of nanosprings induced par the capillary shrinkage. In the case of particulate coatings, the plasticity is essentially related to changes in the microstructure. Moreover, the inhomogeneity of the film should undoubtedly affect the crack healing even if the homogeneity of the nanospring films was not quantified in the present study.

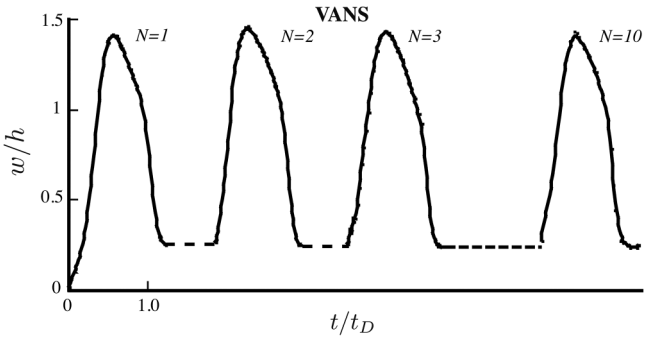

FIG. 11. Measurements of the crack opening and closing of a nanospring film during successive wetting/drying processes ($N = 10$ cycles); the measurements are performed on the same crack.

Finally, the crack opening and closing in nanospring films are remarkably reproducible with subsequent wetting-drying cycles. In this way, a drop of a low-surface-tension solvent is imbibed in a nanospring film then crack formation is induced by the drying process. The same process is repeated several times and the crack opening/closing is measured. The high repeatability of the crack opening/closing is demonstrated in Fig. 11. Here, the duration between two successive cycles is chosen so that the drying process is complete between each cycle; hence, the film of nanosprings becomes dry between each cycle. This behavior can be associated with the mechanical stability of nanospring films under repeated loading tests as shown in Sec. IV C 1.

IV. CONCLUSION

Nanostructured layers made of Vertically Aligned NanoSprings (VANS) are both dense and highly porous materials. Moreover, the high compliance of these films when compared to conventional coatings has been highlighted through nanoindentation testing. Under wetting/drying processes, the film cracks. The resulting crack patterns are similar to those usually observed. However, in the case of VANS, the cracks partially close when the drying process ceases. Based on considerations related to the scale of the film as well as the scale of the individual nanosprings, we have shown that this quasi-healing is associated with the compliance, the weak plasticity, and the high deformability of the individual nanosprings that form the film. Moreover, the mechanical stability of the films has been highlighted through cyclic loading and repeated wetting/drying processes.

SUPPLEMENTARY MATERIAL

See the supplementary material for multicyclic indentation results.

ACKNOWLEDGMENTS

The authors thank Aurore Sibrant for fruitful discussions. This work has benefited from a French State grant BOGUS ('Beads Of colloidal Gel Under Stress') (No. ANR-19-CE06-0030-02) and the U.S. Office of Naval Research (Grant No. N00014-20-1-2433).

AUTHOR DECLARATIONS

Conflict of Interest

The authors have no conflicts to disclose.

DATA AVAILABILITY

The data that support the findings of this study are available from the corresponding author upon reasonable request.

REFERENCES

[1]N. I. Kovtyukhova, B. R. Martin, J. K. N. Mbindyo, P. A. Smith, B. Razavi, T. S. Mayer, and T. E. Mallouk, "Layer-by-layer assembly of rectifying junctions in and on metal nanowires," J. Phys. Chem. B **105**, 8762–8769 (2001).
[2]P. Bakharev, V. Dobrokhotov, and D. McIlroy, "A method for integrating ZnO coated nanosprings into a low cost redox-based chemical sensor and catalytic tool for determining gas phase reaction kinetics," Chemosensors **2**, 56–68 (2014).
[3]X. Duan, J. Wang, and C. M. Lieber, "Synthesis and optical properties of gallium arsenide nanowires," Appl. Phys. Lett. **76**, 1116–1118 (2000).
[4]Z. Tang, N. A. Kotov, and M. Giersig, "Spontaneous organization of single CdTe nanoparticles into luminescent nanowires," Science **297**, 237–240 (2002).
[5]D. McIlroy, D. Zhang, Y. Kranovand, and M. Norton, "Nanosprings," Appl. Phys. Lett. **79**, 1540–1542 (2001).
[6]L. Wang, D. Major, P. Paga, D. Zhang, M. G. Norton, and D. N. McIlroy, "High yield synthesis and lithography of silica-based nanospring mats," Nanotechnology **17**, S298–S303 (2006).
[7]Z. Xia and J. Hutchinson, "Crack patterns in thin films," J. Mech. Phys. Solids **48**, 1107–1131 (2000).
[8]P. Bacchin, D. Brutin, A. Davaille, E. Di Giuseppe, X. D. Chen, I. Gergianakis, F. Giorgiutti-Dauphiné, L. Goehring, Y. Hallez, R. Heyd, R. Jeantet, C. Le Floch-Fouéré, M. Meireles, E. Mittelstaedt, C. Nicloux, L. Pauchard, and M.-L. Saboungi, "Drying colloidal systems: Laboratory models for a wide range of applications," Eur. Phys. J. E **41**, 94 (2018).
[9]S. Sadhukhan, A. Kumar, G. U. Kulkarni, S. Tarafdar, and T. Dutta, "A spring network simulation in three dimensions for designing optimal crack pattern template to fabricate transparent conducting electrodes," Bull. Mater. Sci. **42**, 197 (2019).
[10]J. Walker, "Cracks in a surface look intricately random but actually develop rather systematically," Sci. Am. **255**, 178–183 (1986).
[11]C. Brinker and G. Scherer, *Sol-Gel Science: The Physics and Chemistry of Sol-Gel Processing* (Academic Press, New York, 1990).
[12]A. Atkinson and R. Guppy, "Mechanical stability of sol-gel films," J. Mater. Sci. **26**, 3869–3873 (1991).
[13]A. Groisman and E. Kaplan, "An experimental study of cracking induced by desiccation," Europhys. Lett. **25**, 415–420 (1994).
[14]L. Goehring, W. J. Clegg, and A. F. Routh, "Plasticity and fracture in drying colloidal films," Phys. Rev. Lett. **110**, 024301 (2013).
[15]F. Giorgiutti-Dauphiné and L. Pauchard, "Painting cracks: A way to investigate the pictorial matter," J. Appl. Phys. **120**, 065107 (2016).
[16]D. McIlroy, A. Alkhateeb, D. Zhang, D. Aston, A. Marcy, and M. Norton, "Nanospring formation—unexpected catalyst mediated growth," J. Phys.: Condens. Matter **16**, R415–R440 (2004).
[17]Y. P. Timalsina, D. Oriero, T. Cantrell, T. Prakash, J. Branen, D. E. Aston, K. Noren, J. J. Nagler, S. Rastogi, D. N. McIlroy, and G. Corti, "Characterization of a vertically aligned silica nanospring-based sensor by alternating current impedance spectroscopy," J. Micromech. Microeng. **20**, 095005 (2010).
[18]P. M. Wojcik, P. V. Bakharev, G. Corti, and D. N. McIlroy, "Nucleation, evolution, and growth dynamics of amorphous silica nanosprings," Mater. Res. Express **4**, 015004 (2017).
[19]W. Oliver and G. Pharr, J. Mater. Res. **7**, 1564 (1992).
[20]H. Hirakata, S. Matsumoto, M. Takemura, M. Suzuki, and T. Kitamura, "Anisotropic deformation of thin films comprised of helical nanosprings," Int. J. Solids Struct. **44**, 4030–4038 (2007).
[21]A. F. da Fonseca and D. S. Galvão, "Mechanical properties of nanosprings," Phys. Rev. Lett. **92**, 175502 (2004).
[22]E. Di Giuseppe, A. Davaille, E. Mittelstaedt, and M. François, "Rheological and mechanical properties of silica colloids: From Newtonian liquid to brittle behaviour," Rheol. Acta **51**, 451–465 (2012).
[23]L. Wang, C. Ortiz, and M. C. Boyce, "Mechanics of indentation into micro and nanoscale forests of tubes, rods, or pillars," J. Eng. Mater. Technol. **133**, 011014-1 (2010).
[24]H. Liu, J. Zhai, and L. Jiang, "Wetting and anti-wetting on aligned carbon nanotube films," Soft Matter **2**, 811–821 (2006).
[25]E. Washburn, Phys. Rev. **17**, 273 (1921).
[26]C. Wirth, S. Hofmann, and J. Robertson, "Surface properties of vertically aligned carbon nanotube arrays," Diamond Relat. Mater. **17**, 1518–1524 (2008).
[27]C. Py, R. Bastien, J. Bico, B. Roman, and A. Boudaoud, "3D aggregation of wet fibers," Europhys. Lett. **77**, 44005 (2007).
[28]S. Bohn, L. Pauchard, and Y. Couder, "Hierarchical crack pattern as formed by successive domain divisions." Phys. Rev. E **71**, 046214 (2005).
[29]M. Leang, F. Giorgiutti-Dauphine, L.-T. Lee, and L. Pauchard, "Crack opening: From colloidal systems to paintings," Soft Matter **13**, 5802–5808 (2017).
[30]B. Lawn, *Fracture of Brittle Solids*, 2nd ed., Cambridge Solid State Science Series (Cambridge University Press, 1993).